Applied Acoustics 96 (2015) 180–190

Contents lists available at ScienceDirect

Applied Acoustics

journal homepage: www.elsevier.com/locate/apacoust

Time domain representation of frequency-dependent surface impedance using finite impulse response filters in discrete Huygens' modeling

Renato S.T. de Carvalho *, Arcanjo Lenzi [1], Júlio A. Cordioli [2]

Laboratório de Vibrações e Acústica, Departamento de Engenharia Mecânica, UFSC, Caixa Postal 476, CEP 88040-900 Florianópolis, SC, Brazil

ARTICLE INFO

Article history:
Received 15 February 2014
Received in revised form 20 February 2015
Accepted 11 March 2015
Available online 22 April 2015

Keywords:
Discrete Huygens' Modeling
Sound absorbing materials
Time-domain methods

ABSTRACT

In recent years there has been renewed interest in time-domain numerical methods in view of sound synthesis applications and the need to obtain the impulse response of acoustic systems. Discrete Huygens' Modeling (DHM) is one of the time-domain methods available and it presents interesting characteristics, such as its simple implementation and relatively low computational cost. Although an equivalent method has been widely applied in the field of electromagnetism, its application in the area of acoustics is still limited, especially for describing absorption materials at boundaries. The main aim of this paper is to show the applicability of the Finite Impulse Response (FIR) filters to represent sound absorbing materials in a DHM model, without significantly degrading its computational performance. The DHM have been used to indirectly obtain the frequency response functions of an acoustic cavity, both with and without the presence of absorbing materials on its boundaries. Numerical results and computational times are compared with Finite Element (FE) models of the cavity. While very good agreement between the methods is observed, the computational cost of the DHM models can be orders of magnitude lower than in the case of FE models.

1. Introduction

In 1690, Huygens in his Treatise on Light [1] proposed a theory in which light has a wave-like behavior that allows the position of the wave front at a given future time to be predicted based on its current position. Huygens stated that every point of a wave front may be considered as a center of a secondary disturbance which gives rise to spherical wavelets, and the wave front at any later instant may be regarded as the envelope of these wavelets. This propagation concept can be directly implemented on a digital computer, considering time and space variables in a discretized form. The first discrete form of Huygens' physical model was created with the aim of simulating the wave propagation for two-dimensional cases in the field of electromagnetism [2]. In order to provide the theoretical background, the method was originally proposed using specific concepts of transmission line theory. Since then, the method has been used in other engineering areas, leading to the development of new theoretical approaches. A relatively new approach, called discrete Huygens' modeling (DHM) [3], was conceived with the focus on applications in the area of acoustics. This name directly refers to a discretized form of Huygens' Principle. As stated in [3], the procedure applied is equivalent to the original version published by Johns and Beurle [2], which is known as the Transmission Line Matrix Method (TLM). Unlike traditional methods, such as Finite Difference and Finite Element, in which a discretization procedure is applied to a mathematical model [4], DHM may be considered as a physical approach, since it does not involve the representation of the problem by a differential equation in order to model it [5]. The main idea of the method is to directly obtain algebraic equations in a discretized domain, based on the following fundamental laws of physics [4–9]: conservation of mass, conservation of momentum, conservation of energy and field continuity conditions. In DHM, the analyzed domain is divided into sub-domains in order to individually apply the conservation laws. In acoustic applications, basic units or nodes of the mesh are formed from intersections of virtual tubes. The result is a so-called DHM node with a given number of branches and an impedance discontinuity in the center connecting all branches, defining the control volume. A DHM mesh is defined by connecting node branches with branches from adjacent nodes. These branches have the function of a waveguide and the propagation occurs when an incident wave signal travels to the node center through one of the branches and, by following the

* Corresponding author. Tel.: +55 48 3721 9227x219.
E-mail addresses: renato@lva.ufsc.br (R.S.T. de Carvalho), arcanjo@lva.ufsc.br (A. Lenzi), julio.cordioli@ufsc.br (J.A. Cordioli).
[1] Tel.: +55 48 3721 9227x202.
[2] Tel.: +55 48 3721 9227x203.

http://dx.doi.org/10.1016/j.apacoust.2015.03.003
0003-682X/

conservation principles, the signal scatters throughout the branches of the node. The signal travels towards the adjacent nodes and, in the next time step, adds its amplitude to pulses coming from other sections of the mesh. In general, real acoustic boundaries are frequency-dependent, which means that the reflected wave differs both in terms of phase and amplitude in relation to the incident wave for each analyzed frequency [10]. This is especially important for the representation of absorbing materials in acoustics and this is a particular aspect of the DHM theory that is still not sufficiently developed. The simplest approach would be to transform the impedance values into the time domain and then perform a convolution with the incoming signals [11]. However, this approach has a prohibitive computational cost [12]. Hence, most authors use a single reflection coefficient to represent the boundary condition in DHM simulations [3], which limits the DHM application to frequency-independent materials. Different attempts to model frequency-dependent materials in the time domain in a more efficient way can be found in the literature [11,13–15]. In [11], a polynomial fit was used to model the frequency-domain impedance, while in [13] an approximation of the impedance as the sum of linear systems was adopted. In [14] FIR coefficients were used to model the atmospheric absorption. The approach in [15] led to an FD–TD impedance boundary condition method, considering two types of boundaries, that is, with spring-like or mass-like behavior. In summary, the material reflection factor may have either a single value, allowing the analysis of a single frequency for each simulation run, or a set of coefficients related to the material impulse response. The latter case enables a multi-frequency analysis for each simulation run. Hence, a kind of truncated impulse response (small size array) needs to be obtained in order to establish how the absorbing material behaves in the time domain. In the present paper, this was achieved in an efficient programming manner by using FIR digital filter coefficients that must be convolved with the incident signal. Many works [12,16–19] have been developed to compare DHM/TLM to traditional methods, both in terms of theoretical approaches and computational performance. In this paper, a considerably better performance has been achieved by the DHM algorithm when compared to an equivalent solution for the Finite Element method in the frequency domain. Additionally, a DHM scattering matrix derivation for a homogeneous and non-dissipative medium is also described in the next section in a step by step manner, since even reference publications such as [3,5] do not detail some specific aspects that are covered in this paper, such as the physical assumptions applied and the particle velocity derivation.

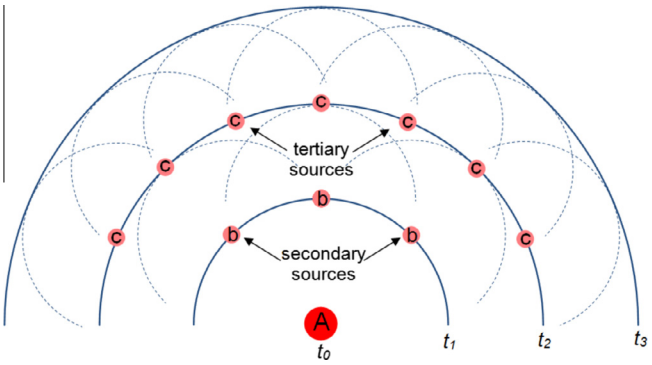

Fig. 1. Representation of Huygens' physical model.

2. Fundamental concepts of discrete Huygens' modeling

As proposed by Huygens [1], the wave front propagation may be represented as the superposition of an infinite number of point sources, each one radiating spherical wavelets, as shown in Fig. 1. The light from point A is spherically expanded, producing the wave front, where each point of this front behaves as if it were a new light wave source. The secondary sources (b), starting from the wave front at time step t_1, create wavelets that form a new wave front, which, in turn, have further tertiary sources (c), yielding a new wave front at time step t_2, and so on. Through this physical model of propagation it is possible to predict a future position of the wave front from its current position.

The basic idea of discrete Huygens' modeling consists of breaking down the continuous domain shown in Fig. 1 into sub-domains in order to apply the Huygens Principle and the conservation laws individually. Fig. 2 shows a signal propagation sequence in a two-dimensional mesh obtained from dividing the continuous domain into discrete elements (nodes). As a consequence, a node network is formed with space discretization steps $\Delta x = \Delta y = \Delta l$, enabling the sound field to propagate throughout the mesh at discrete times $t_d = k\Delta t$.

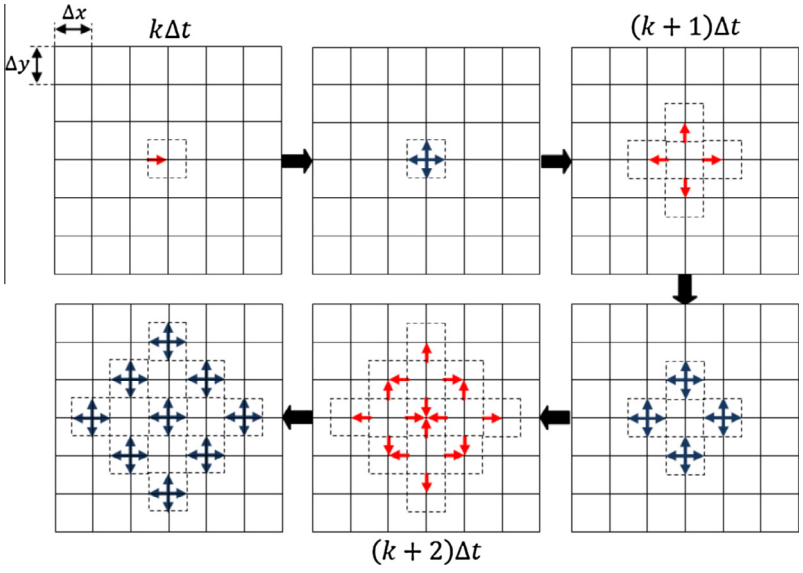

Fig. 2. Example of a signal propagation sequence in a 2D acoustic mesh.

The propagation mechanism consists of an incident sound pressure signal (in red) arriving at an arbitrary node in a discrete time $k\Delta t$. This creates scattered signals (in blue), where part is transmitted and part is reflected back, which become new incident signals at the adjacent nodes in the next discrete time $(k+1)\Delta t$. The process goes on until the simulation ends.

The key point of the method is the calculation of the scattered signals, which is carried out based on a scattering matrix. In electromagnetism, the scattering matrix is derived using laws and concepts from transmission line theory, which guarantee the conservation of charge and energy. A similar procedure can be used in acoustics. However, in this study, a more straightforward approach is applied to a two-dimensional lossless acoustic waveguide. It should be noted that the same procedure can be expanded to three-dimensional cases or topologies that consider losses and anisotropic behavior.

In the following derivation, an acoustic wave is considered to be propagating through a waveguide and scattering at a discontinuity called a *junction*, with the following physical assumptions: the fluid is homogeneous, inviscid, isotropic and with no thermal conductivity; there is uniform sound speed when acoustic plane waves cross the control volume boundary where $\Delta l \ll \lambda$; there is no mass or energy source within the control volume; and gravitational forces are neglected.

A *two-dimensional lossless acoustic node* is defined by four orthogonal tubular branches with arbitrary specific acoustic impedances (Z_1; Z_2; Z_3; Z_4) and cross-sectional areas (S_1; S_2; S_3; S_4), as shown in Fig. 3. In the shared region between branches, a fixed discrete control volume (CV), called the node center, is defined. Since the wavelength of the propagating wave is assumed to be much larger than the largest characteristic dimension of the node, the reference point can be placed at the midpoint ($x = 0$, $y = 0$) of the control volume (CV).

The incident pressure waves in each branch p_b^i (with b from 1 to 4) are assumed to have a harmonic time variation and an amplitude P_b^i, such that

$$\begin{aligned} p_1^i(x,t_d) &= P_1^i \exp[j(\kappa x - \omega t_d)], \\ p_2^i(x,t_d) &= P_2^i \exp[j(-\kappa y - \omega t_d)], \\ p_3^i(y,t_d) &= P_3^i \exp[j(-\kappa x - \omega t_d)], \\ p_4^i(y,t_d) &= P_4^i \exp[j(\kappa y - \omega t_d)]. \end{aligned} \tag{1}$$

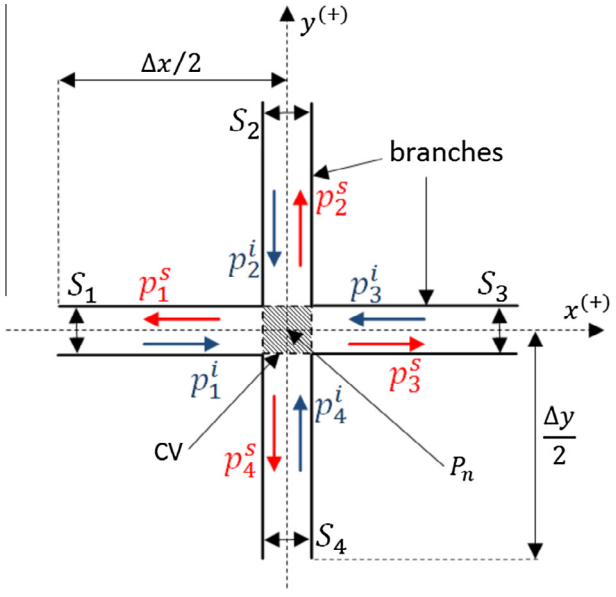

Fig. 3. Incident and scattered waves in a 2D acoustic lossless node.

The waves encounter a change in the acoustic impedance when the propagation tube breaks down into other branches. Therefore, each incident wave gives rise to four scattered pressure waves p_{b1}^s, p_{b2}^s, p_{b3}^s, p_{b4}^s. One is reflected back through the incident branch and three are transmitted through the other ones. The sum of all scattered waves in one branch $(p_{b1}^s + p_{b2}^s + p_{b3}^s + p_{b4}^s)$ due to each incident signal p_b^i, results in the total scattered signal in one branch p_b^s given by

$$\begin{aligned} p_1^s(x,t_d) &= P_1^s \exp[j(-\kappa x - \omega t_d + \emptyset)], \\ p_2^s(x,t_d) &= P_2^s \exp[j(\kappa y - \omega t_d + \emptyset)], \\ p_3^s(y,t_d) &= P_3^s \exp[j(\kappa x - \omega t_d + \emptyset)], \\ p_4^s(y,t_d) &= P_4^s \exp[j(-\kappa y - \omega t_d + \emptyset)], \end{aligned} \tag{2}$$

where P_b^s is the scattered wave amplitudes in a branch b, $j = \sqrt{-1}$ is the imaginary unity, $\kappa = \omega/c$ is the wavenumber, ω is the angular frequency, c is the phase velocity, $t_d = k\Delta t$ is the discrete time, $\emptyset$ is the phase angle and x and y are the Cartesian coordinates.

Once the pressure waves are defined, the scattering matrix can be obtained by applying the following fundamental laws of physics to the defined control volume [4,5,13] in a given discrete time $k\Delta t$:

1. Conservation of mass

The net mass flow through the control surface defined by the node center ($x = 0$, $y = 0$) must be equal to zero, leading to

$$\rho\left[\left(U_1^i + U_1^s\right) + \left(U_2^i + U_2^s\right) + \left(U_3^i + U_3^s\right) + \left(U_4^i + U_4^s\right)\right] = 0, \tag{3}$$

where ρ is the mass density and U_b^i and U_b^s are the volume velocities of the incident and scattered waves in each branch. Since the acoustic impedance can be defined as $z = p/U = p/uS = Z/S$, where u is the particle velocity, Eq. (3) can be rewritten in terms of sound pressure waves p and specific acoustic impedances Z

$$\rho\left[S_1\left(\frac{p_1^i}{Z_1} - \frac{p_1^s}{Z_1}\right) + S_2\left(\frac{p_2^i}{Z_2} - \frac{p_2^s}{Z_2}\right) + S_3\left(\frac{p_3^i}{Z_3} - \frac{p_3^s}{Z_3}\right) + S_4\left(\frac{p_4^i}{Z_4} - \frac{p_4^s}{Z_4}\right)\right] = 0. \tag{4}$$

Assuming that the *two-dimensional lossless node* has identical geometrical characteristics implies that $S_1 = S_2 = S_3 = S_4 = S_g$. Thus, the conservation of mass equation becomes

$$\frac{p_1^i - p_1^s}{Z_1} + \frac{p_2^i - p_2^s}{Z_2} + \frac{p_3^i - p_3^s}{Z_3} + \frac{p_4^i - p_4^s}{Z_4} = 0. \tag{5}$$

2. Continuity of the sound pressure field

The sound pressure at node p_n must be equal for all branches in the Cartesian position $x = 0$, $y = 0$, so that

$$\begin{aligned} p_n &= p_1^i + p_1^s, \\ p_n &= p_2^i + p_2^s, \\ p_n &= p_3^i + p_3^s, \\ p_n &= p_4^i + p_4^s. \end{aligned} \tag{6}$$

These expressions are rearranged in terms of each of the unknown scattered waves. Starting with the scattered wave p_1^s, one obtains

$$\begin{aligned} p_2^s &= p_1^i + p_1^s - p_2^i, \\ p_3^s &= p_1^i + p_1^s - p_3^i, \\ p_4^s &= p_1^i + p_1^s - p_4^i. \end{aligned} \tag{7}$$

Substituting Eqs. (1), (2) and (7) into Eq. (5) and considering the Cartesian position ($x = 0$; $y = 0$) and $\emptyset = 0$, the following expression in terms of scattered pressure amplitudes and admittance ($Y = 1/Z$) is obtained:

$$P_1^s = \frac{(Y_1 - Y_2 - Y_3 - Y_4)P_1^i + 2Y_2P_2^i + 2Y_3P_3^i + 2Y_4P_4^i}{(Y_1 + Y_2 + Y_3 + Y_4)}. \tag{8}$$

Assuming an isotropic scattering, where the admittance is the same for all branches ($Y_1 = Y_2 = Y_3 = Y_4 = Y_g$), one obtains the first equation for a *two-dimensional lossless node*:

$$4P_1^s = -2P_1^i + 2P_2^i + 2P_3^i + 2P_4^i. \tag{9}$$

This expression relates the scattered wave in one branch to the incident waves from all branches. If the same procedure is applied to the other scattered signals (p_2^s, p_3^s, p_4^s), a set of equations is established as follows

$$\begin{aligned} 4P_1^s &= -2P_1^i + 2P_2^i + 2P_3^i + 2P_4^i, \\ 4P_2^s &= +2P_1^i - 2P_2^i + 2P_3^i + 2P_4^i, \\ 4P_3^s &= +2P_1^i + 2P_2^i - 2P_3^i + 2P_4^i, \\ 4P_4^s &= +2P_1^i + 2P_2^i + 2P_3^i - 2P_4^i. \end{aligned} \tag{10}$$

This set of equations is valid for all nodes of the mesh. Considering a homogeneous isotropic medium and a lossless node, the system of equations can be represented in a matrix form as

$$\begin{Bmatrix} P_1^s \\ P_2^s \\ P_3^s \\ P_4^s \end{Bmatrix}_k^n = \frac{1}{2}\begin{bmatrix} -1 & +1 & +1 & +1 \\ +1 & -1 & +1 & +1 \\ +1 & +1 & -1 & +1 \\ +1 & +1 & +1 & -1 \end{bmatrix} \begin{Bmatrix} P_1^i \\ P_2^i \\ P_3^i \\ P_4^i \end{Bmatrix}_k^n, \tag{11}$$

or $${}_k^n\mathbf{p}^s = \mathbf{S}_k^n\mathbf{p}_i, \tag{12}$$

where ${}_k^n\mathbf{p}^s$ and ${}_k^n\mathbf{p}^i$ are vectors representing the scattered and incident pressures, respectively, in each of the four branches of $n(x_d, y_d)$ mesh nodes at a discrete time $k\Delta t$ and $\mathbf{S}$ is the scattering matrix.

The scattering matrix can be considered as the base of wave propagation in DHM, since it defines the way the scattering process occurs. It determines if there are losses, medium changes or if the material exhibits a frequency-dependent and non-isotropic behavior. It is worth noting that the same equations can be obtained when performing the balance of momentum and energy carried out by the fluid through the control volume, since all properties associated with a fluid are subjected to the conservation principles.

As a consequence of the field continuity principle, the resulting amplitude of the sound pressure ${}_k^nP$ at the center of the node is the sum of the incident and scattered wave amplitudes for each branch. This can be easily obtained by substituting Eq. (8) in Eq. (6), which gives

$${}_k^nP = \frac{(2{}_k^nP_1^iY_1 + 2{}_k^nP_2^iY_2 + 2{}_k^nP_3^iY_3 + 2{}_k^nP_4^iY_4)}{(Y_1 + Y_2 + Y_3 + Y_4)}. \tag{13}$$

Since $Y_1 = Y_2 = Y_3 = Y_4 = Y_g$, Eq. (13) can be simplified and the sound pressure at the center of the node is obtained using

$${}_k^nP = \frac{{}_k^nP_1^i + {}_k^nP_2^i + {}_k^nP_3^i + {}_k^nP_4^i}{2}. \tag{14}$$

The particle velocity components at an arbitrary node n and in a given discrete time $k\Delta t$ are obtained by applying the momentum conservation principle in the x and y directions, inspired by the magnetic flow conservation [6] in electromagnetism, which gives the following expressions:

$${}_k^nV_x\left(\sum_{i=1,3}\rho_iS_i\right) = \sum_{i=1,3}{}_k^nV_i\rho_iS_i = \frac{{}_k^nP_1^i - {}_k^nP_1^S}{Z_1}\rho_1S_1 + \frac{{}_k^nP_3^S - {}_k^nP_3^i}{Z_3}\rho_3S_3, \tag{15}$$

$${}_k^nV_y\left(\sum_{i=2,4}\rho_iS_i\right) = \sum_{i=2,4}{}_k^nV_i\rho_iS_i = \frac{{}_k^nP_2^s - {}_k^nP_2^i}{Z_2}\rho_2S_2 + \frac{{}_k^nP_4^i - {}_k^nP_4^s}{Z_4}\rho_4S_4. \tag{16}$$

Describing the scattered signal in terms of the incident signal by using Eq. (10), as well as considering the simplifications associated to the *two-dimensional lossless node*, one obtains:

$${}_k^nV_x = \frac{{}_k^nP_1^i - {}_k^nP_3^i}{Z_g}, \tag{17}$$

$${}_k^nV_y = \frac{{}_k^nP_4^i - {}_k^nP_2^i}{Z_g}. \tag{18}$$

Finally, the following set of expressions is required to establish the connections and propagation of the acoustic signal between nodes:

$$\begin{aligned} {}_k^nP_1^i(x_d + 1, y_d) &= {}_{k-1}^nP_3^s(x_d, y_d), \\ {}_k^nP_2^i(x_d, y_d - 1) &= {}_{k-1}^nP_4^s(x_d, y_d), \\ {}_k^nP_3^i(x_d - 1, y_d) &= {}_{k-1}^nP_1^s(x_d, y_d), \\ {}_k^nP_4^i(x_d, y_d + 1) &= {}_{k-1}^nP_2^s(x_d, y_d), \end{aligned} \tag{19}$$

where x_d and y_d are the discretized Cartesian node positions. The expressions in (19) are represented in Fig. 4, which illustrates that each of the scattered signals of an arbitrary node n, at the previous time step $(k-1)\Delta t$, will become incident signals on their adjacent nodes in the current time step $k\Delta t$.

It should be noted that all expressions for a *two-dimensional lossless node* can be extrapolated to a generic node having any number of branches, with losses and also considering an anisotropic behavior, as shown in [3,20,21]. In this particular study, a

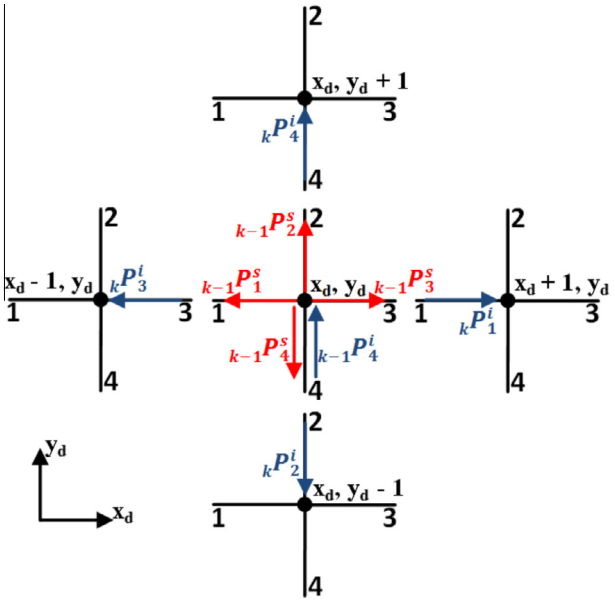

Fig. 4. Connections between nodes via branches.

three-dimensional lossless scalar node [22] have been used for the internal nodes, following the scattering equation

$$\begin{Bmatrix} P_1^s \\ P_2^s \\ P_3^s \\ P_4^s \\ P_5^s \\ P_6^s \end{Bmatrix}^n_k = \frac{1}{3}\begin{bmatrix} -2 & +1 & +1 & +1 & +1 & +1 \\ +1 & -2 & +1 & +1 & +1 & +1 \\ +1 & +1 & -2 & +1 & +1 & +1 \\ +1 & +1 & +1 & -2 & +1 & +1 \\ +1 & +1 & +1 & +1 & -2 & +1 \\ +1 & +1 & +1 & +1 & +1 & -2 \end{bmatrix} \begin{Bmatrix} P_1^i \\ P_2^i \\ P_3^i \\ P_4^i \\ P_5^i \\ P_6^i \end{Bmatrix}^n_k, \tag{20}$$

and for boundary adjacent nodes, the connection process is described in the next section.

3. DHM implementation of boundary conditions using FIR filter coefficients

A rigid boundary condition can be easily implemented in DHM by assuming that the incident wave in a boundary adjacent node at a time step $k\Delta t$ is the scattered wave at a previous time step $(k-1)\Delta t$ at the same node followed by a reflection at the boundary. However, the representation of a boundary with a sound absorbing material is more complex, since the material may display a resistive and reactive behavior. A first simplification may be made by assuming that the material can be properly represented by a locally-reacting surface (LRS) impedance, which means that the scattered wave at a given branch reaching the boundary is not influenced by incident waves at other branches, and is dependent only on the incident wave at that branch. This assumption is generally accepted for several acoustic materials and thin layers [23].

A second simplification would be considering a constant impedance value at the surface. However, sound absorbing materials are usually frequency-dependent. The simplest way to solve this issue would be to transform the impedance data into the time domain and obtain the impulse response. A drawback associated with this approach is the high computational demand when performing the convolution operation. As stated by [11], approximating the impedance data through a polynomial of low order greatly reduces the computational effort. Another approach involves the approximation of the sound impedance as a sum of linear systems [13], which allows the expression of the time-domain impedance as a decaying exponential series and thus the use of a recursive convolution method to numerically solve the reflection process.

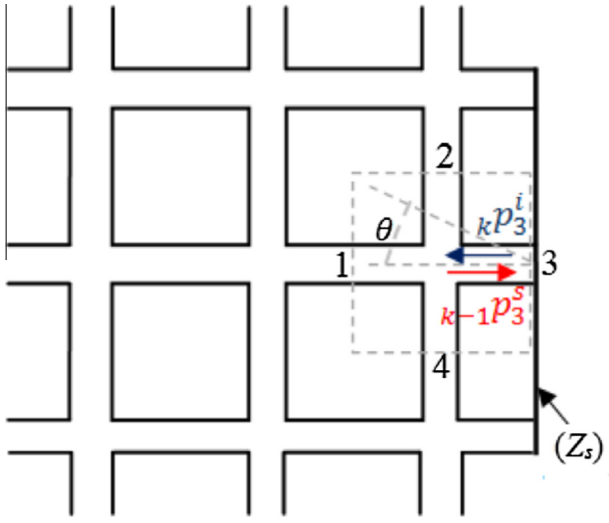

Fig. 5. Boundary impedance representation.

In the present paper, it is proposed that the absorbent behavior of the material is taken into account by considering a set of reflection factor values in the time domain, based on its complex acoustic impedance. To better explain the procedure, the DHM reflection mechanism is summarized in Fig. 5. The scattered pressure signal $_{k-1}p_3^s$, propagates towards the boundary after the scattering process at the adjacent node in a previous time step $k-1$. As the signal reaches it, part is reflected back proportionally with the reflection factor, resulting in an incident pressure signal $_kp_3^i$ at the boundary adjacent node in the current step k.

The reflection factor Γ_s can be written for any angle of incidence θ considering the ratio between the reflected and incident signals at the boundary as in [5,10,24,25]

$$\Gamma_s(\theta) = \frac{p_s^r}{p_s^i} = \frac{Z_s \cos\theta - Z_g}{Z_s \cos\theta + Z_g} = \frac{{}_kp_3^i}{{}_{k-1}p_3^s}, \tag{21}$$

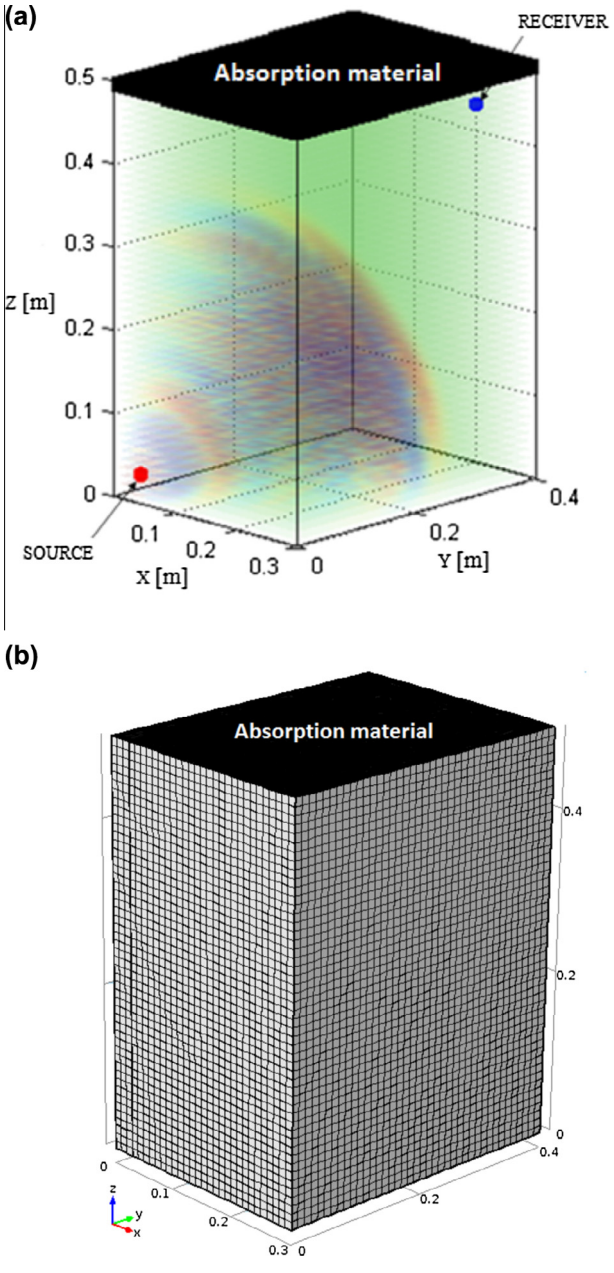

Fig. 6. Cavity (physical system) and mesh for FEM–FD and DHM–TD. (a) Physical system and (b) mesh applied in both methods.

where Z_s and Z_g are respectively the surface and waveguide impedances.

If the surface impedance is independent of the incident angle then a locally reacting surface is being assumed, which means that the particle velocity at the surface is unaffected by pressures other than those in the immediate vicinity of the point of interest [26]. As a consequence, adjacent sections of the same wall surface are mutually independent and no tangential waves are transmitted along the wall surface [10,15]. Thus, the following simplified version of the reflection factor is obtained and used in the implemented algorithm:

$$\Gamma_s = \frac{Z_s - Z_g}{Z_s + Z_g}, \tag{22}$$

as well as the absorption coefficient

$$\alpha = 1 - |\Gamma_s|^2. \tag{23}$$

From the reflection factor, the connection process for a boundary adjacent node is carried out using

$${}^{n}_{k}P^{i} = \Gamma_{s_{(k-1)}}\, {}^{n}_{k}P^{s}. \tag{24}$$

Table 1
Cavity model information (FEM–FD and DHM–TD).

Parameters	Values
Cavity dimensions (m)	$0.3 \times 0.4 \times 0.5$
Node dimensions (m)	$0.01 \times 0.01 \times 0.01$
Number of nodes	60,000 ($30 \times 40 \times 50$)
Source position (m)	S (0.03; 0.03; 0.03)
Receiver position (m)	R (0.25; 0.35; 0.45)

Table 2
Simulation data synthesis – rigid cavity.

Parameters	Values
Simulation time	0.5 s
Time step (Δt)	$\cong 1.68 \times 10^{-5}$ s
Number of iterations	29,741
Frequency step (Δf)	2 Hz
Cut-off frequency	3434 Hz
Volume velocity ($\hat{U}$)	$1e^{-5}$ m^3/s
CPU time	DHM $\cong$ 255 s FEM $\cong$ 16,200 s

Note: Intel processor Core (TM) i7 CPU @ 2.93 GHz 6 GB RAM, Windows 64 bits.

Considering the boundaries as ideal systems and establishing an analogy with the version of the method used in electromagnetism studies, the impedance, reflection factor and absorption coefficient can assume the following extreme values [4,5,7,9,10,13]:

1. $Z_s \ll Z_g$; $\Gamma_s \to -1$; $\alpha \to 0$, modeling a "soft wall/pressure-release" or short circuit (perfect conductor in electromagnetism), resulting in a reflected wave in antiphase with the incident wave (e.g.: water–air interface);
2. $Z_s \gg Z_g$; $\Gamma_s \to 1$; $\alpha \to 0$, modeling a "hard wall" or open circuit (magnetic wall in electromagnetism), resulting in a reflected wave completely in phase with the incident wave;
3. $Z_s = Z_g$; $\Gamma_s = 0$; $\alpha = 1$, modeling an impedance matching or open space (free field), which results in a complete absorption of the incident wave. It is worth to point out that such a condition induces instabilities [27] and experience has shown that significant improvements can be obtained by using absorbing layers [5].

The material impedance may have either a single value in the time domain, allowing analysis of a single frequency for each simulation run, or a set of coefficients related to the impulse response of frequency-dependent materials. The latter case enables a multi-frequency analysis in a single DHM simulation run. It is ideally represented for causal systems by a discrete convolution between incident signals and the material impulse response $h(m)$ given by

$${}^{n}_{k}P^{i} = \sum_{m=0}^{\infty} h(m)_{(k-1-m)}\, {}^{n}_{}P^{s}. \tag{25}$$

An alternative approach can be applied using an FIR filter to represent the material frequency dependency in the time domain. This filter is characterized by a *difference equation* or a filtered response $y(k)$ obtained from a linear combination of previous and current values of the input signal $x(k)$. Thus, the output signal $y(k)$ obtained from the FIR filter is given by a discrete convolution between the input signal and the filter coefficients [28–30], as follows

$$y(k) = \sum_{m=0}^{N} h_m x(k-m), \tag{26}$$

where N is the filter order, $x(k)$ is the input signal, h_m are the filter coefficients and $y(k)$ is the output signal for a given time step k.

As shown in Fig. 5, the boundary reflected signal becomes the incident sound pressure ${}^{n}_{k}P^{i}$ at the adjacent node, which numerically corresponds to the filter output signal $y(k)$. The reflection

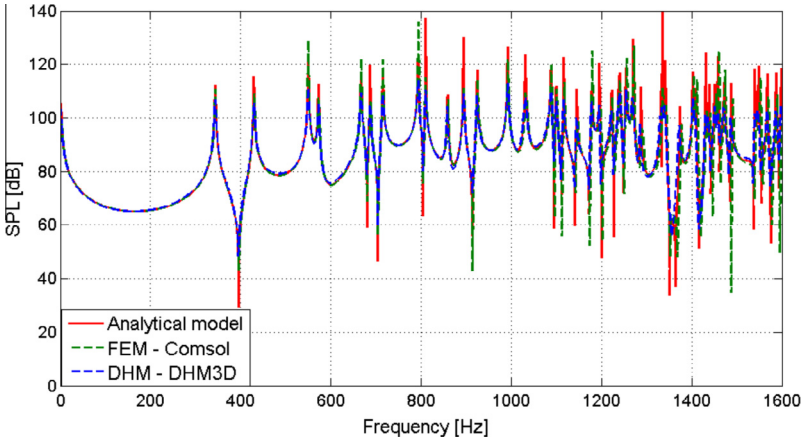

Fig. 7. Frequency response – rigid cavity.

factor array $\mathbf{\Gamma_s}$ is represented in the time domain by $N+1$ coefficients h_m of an FIR filter. The advantage of the proposed approach is the reduced number of coefficients necessary to obtain the required accuracy in the material representation when compared to the full convolution procedure. Although the $N+1$ last scattered sound pressures from the $N+1$ previous time iterations must be stored for an Nth order digital filter, the DHM implemented algorithm in Matlab® is able to perform the operation given by Eq. (26) for any boundary region (set of nodes), with a reduced computational cost when compared to other numerical approaches. Therefore, Eq. (26) becomes

$$ {}^{n}_{k}P^{i} = \sum_{m=0}^{N} h_m \, {}^{n}_{(k-1-m)}P^{s}. \tag{27} $$

In this paper, filter design techniques have been used to indirectly obtain time domain reflection factor values (filter coefficients) by using as the reference data the surface impedance values in the frequency domain provided by the analytical model [23,31], summarized as

$$ \widetilde{Z}_s(\omega) = -j\widetilde{Z}_c(\omega)\cot(\tilde{k}_c(\omega)L), \tag{28} $$

where $\widetilde{Z}_c(\omega) = [\widetilde{\rho}_{ef}\widetilde{K}_{ef}]^{1/2}$ and $\tilde{k}_c(\omega) = \omega[\widetilde{\rho}_{ef}/\widetilde{K}_{ef}]^{1/2}$ are the characteristic impedance and wavenumber, respectively, $j=\sqrt{-1}$ is the imaginary unity, L is the sample length, $\tilde{\rho}_{ef}$ is the effective density, $\widetilde{K}_{ef} = \gamma P_0/\tilde{\beta}$ is the effective bulk modulus, γ is the specific heat ratio, P_0 is the medium static pressure and $\tilde{\beta}$ is the compressibility factor. Thus, based on the work of Johnson et al. [32] and Lafarge et al. [33] the expressions for the effective density and effective bulk modulus, respectively, are given by:

$$ \tilde{\rho}_{ef}(\omega) = \rho_0\alpha_\infty\left(1+\frac{\phi\eta}{j\omega\rho_0\alpha_\infty q_0}\left(1+j\frac{4\omega\rho_0 q_0^2\alpha_\infty^2}{\eta\phi^2\Lambda^2}\right)^{\frac{1}{2}}\right), \tag{29} $$

$$ \widetilde{K}_{ef}(\omega) = \frac{\gamma P_0}{\gamma-(\gamma-1)\left(1+\frac{\phi\eta}{j\omega\rho_0 \mathrm{Pr} q_0'}\left(1+j\frac{4\omega\rho_0 \mathrm{Pr} q_0'^2}{\eta\phi^2\Lambda'^2}\right)^{\frac{1}{2}}\right)^{-1}}, \tag{30} $$

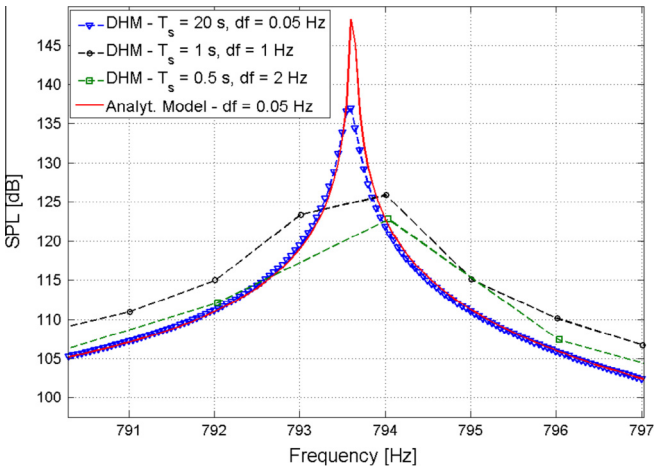

Fig. 8. Frequency shifts for different spectral discretization.

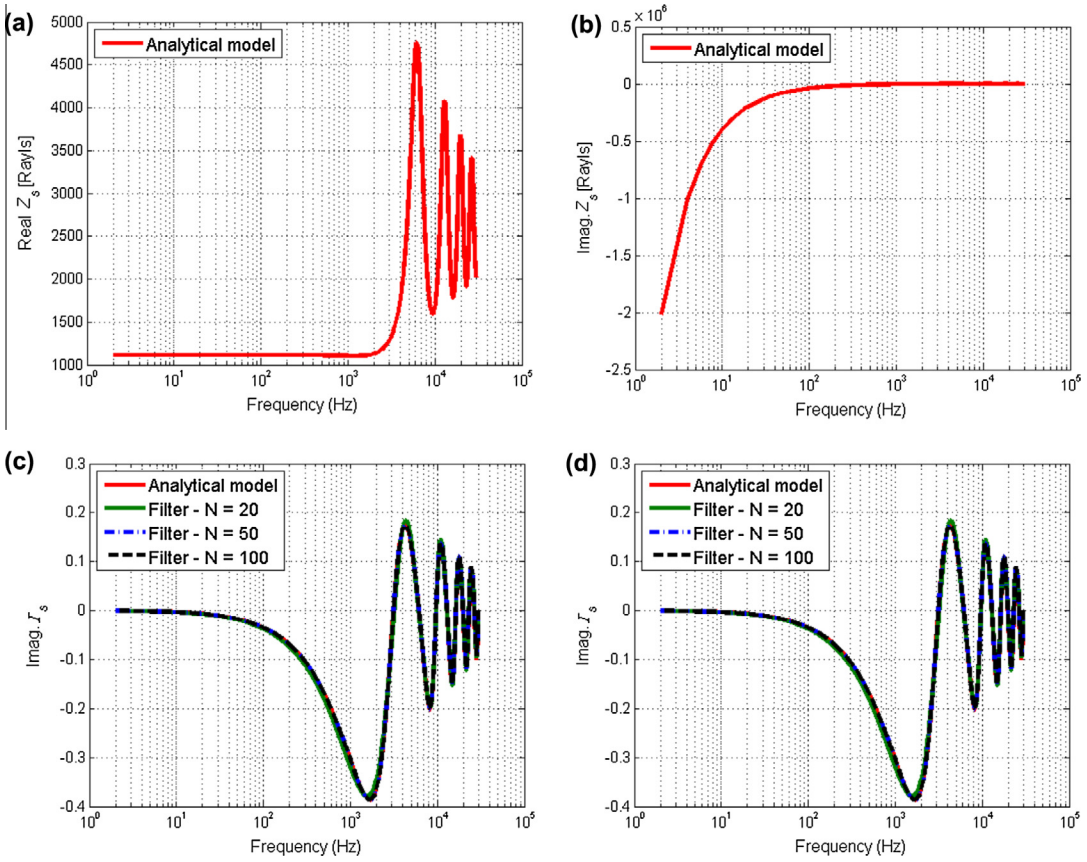

Fig. 9. Surface impedance and reflection factor in frequency domain – fictitious material. (a) Impedance – real part, (b) impedance – imag. part, (c) reflection factor – real part and (d) reflection factor – imag. part.

where α_∞ is the tortuosity, ϕ is the porosity, η is the fluid viscosity, ρ_0 is the medium density, q_0 is the viscous permeability, q'_0 is the thermal permeability, Pr is the Prandtl number, Λ is the viscous characteristic length and Λ' is the thermal characteristic length.

The surface impedance values from Eq. (28) are converted to reflection factor values using Eq. (22) and then FIR filter coefficients are calculated using the least-squares method [34] provided by a 'Guided User Interface' namely 'FilterBuilder' from the software Matlab®. The best fit in the least-squares method minimizes the sum of squared residuals, where a residual is the difference between an observed value and the desired value provided by measured data or, in this paper, the analytical model shown in Eq. (28). This technique is applicable to any arbitrary frequency response and the results obtained from the application of this concept are discussed in the next section.

4. Numerical results

4.1. Model characterization

In order to validate the discrete Huygens' method described in the previous section, an acoustic cavity was simulated both with and without considering an acoustic material applied to its boundary. Firstly, in Section 4.2, an analytical model and a finite element model (direct approach) of the cavity with no damping are used to validate the DHM results. In Sections 4.3 and 4.4, when considering acoustic materials, five of the cavity faces are defined as rigid, while for one face (upper face), the boundary condition is defined based on complex impedance values in FEM–FD (Finite Element Method–Frequency Domain) and the corresponding reflection factor values in DHM–TD (discrete Huygens' modeling–Time Domain) simulations. The physical system and the mesh are illustrated in Fig. 6 and detailed in Table 1.

The simulation parameters for all cases presented are obtained by firstly defining the maximum or cut-off frequency f_c that needs to be analyzed in the application. Once this information is known, the required spatial resolution can be calculated using the criterion $\Delta l \leqslant 0.1c/f_c$ [2,5,6,9]. As a consequence, the adopted time interval can be obtained using the expression $\Delta t = \Delta l/v_g$, where $v_g = c\sqrt{3}$ is the waveguide velocity [35]. The definition of the spatial resolution could also be the starting point.

A monopole sound source (in red[3] – Fig. 6a) was considered in both models and placed at coordinate S (0.03; 0.03; 0.03). As stated in [2,9], a source excitation can be a time-dependent function, a Gaussian pulse, or more often an Impulse, which ideally contains infinite frequencies of the spectrum. It means that one simulation run contains all the necessary information about the frequency response for frequencies from zero to infinity. In practice, the mesh itself has a filtering effect, where the frequency response has an upper limit that depends on the coarseness of the mesh, which means it will have an acceptable accuracy for frequencies below the cut-off frequency f_c.

The receiver (in blue – Fig. 6a) was placed close to the corner opposite the source, at coordinate R(0.25; 0.35; 0.45), seeking to maximize the intensity of the acoustic modes in the impulse response function. From the DHM impulse response function it is possible to obtain via FFT – Fast Fourier Transform, transfer functions between the source and the receiver point for the acoustic field established inside the cavity.

4.2. Rigid cavity

In order to reinforce the process used for the validation of the DHM–TD implemented code, firstly an FEM–FD model and an analytical model were used as references and compared with DHM–TD considering all cavity faces as rigid walls. Together with the FEM–FD model, an analytical model was also used to validate the results. The model is based on the expansion of the cavity modes as given in [10,36],

$$p(x,y,z,t) = \rho c^2 \widehat{U} \sum_{i=0}^{I}\sum_{j=0}^{J}\sum_{k=0}^{K} \frac{\omega \Psi_{ijk}(x,y,z)\Psi_{ijk}(x_0,y_0,z_0)}{V_{ijk}(\omega^2-\omega_{ijk}^2)} \times \cos(\omega t + \phi - \pi/2), \quad (31)$$

where ρ and c are the medium density and sound speed, respectively, $\widehat{U}$ is the volume velocity, Ψ_{ijk} and $f_{ijk} = \omega_{ijk}/2\pi$ are the mode shapes and natural frequencies, respectively, V_{ijk} is the modal volume and i, j, k are the modal indexes in each Cartesian direction.

The data synthesis for this particular simulation is detailed in Table 2. The lossless implemented code takes round 255 s to complete the simulation, including the application of the FFT. Therefore, the DHM–TD processing time is approximately 63 times faster than the FEM–FD simulation.

Fig. 7 shows the results for the frequency responses $H(K)$ obtained by FEM–FD (Comsol v4.3®), DHM–TD (Matlab® algorithm) and the analytical model. As a consequence of the simulation time, $t_s = 0.5$ s, a frequency step $\Delta f = 2$ Hz is obtained.

The spectral discretization leads to amplitude differences for each method, especially in the region where the resonance frequencies are located. As the resonance is a peak of the spectrum amplitude, even small shifts in frequency can result in differences in

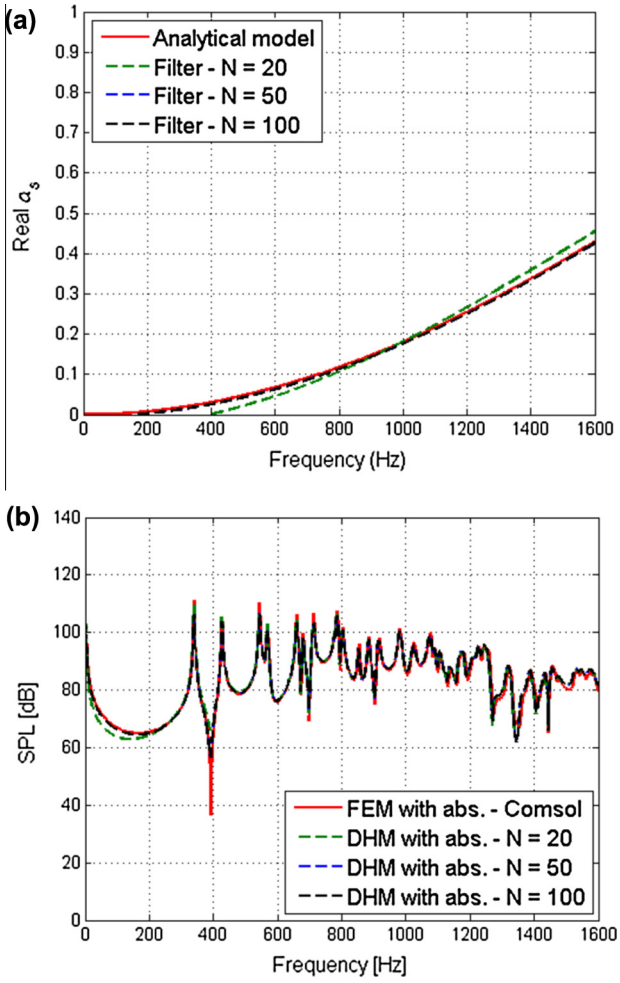

Fig. 10. Frequency response after applying the fictitious material. (a) Absorption coefficient and (b) frequency response.

[3] For interpretation of color in Fig. 6, the reader is referred to the web version of this article.

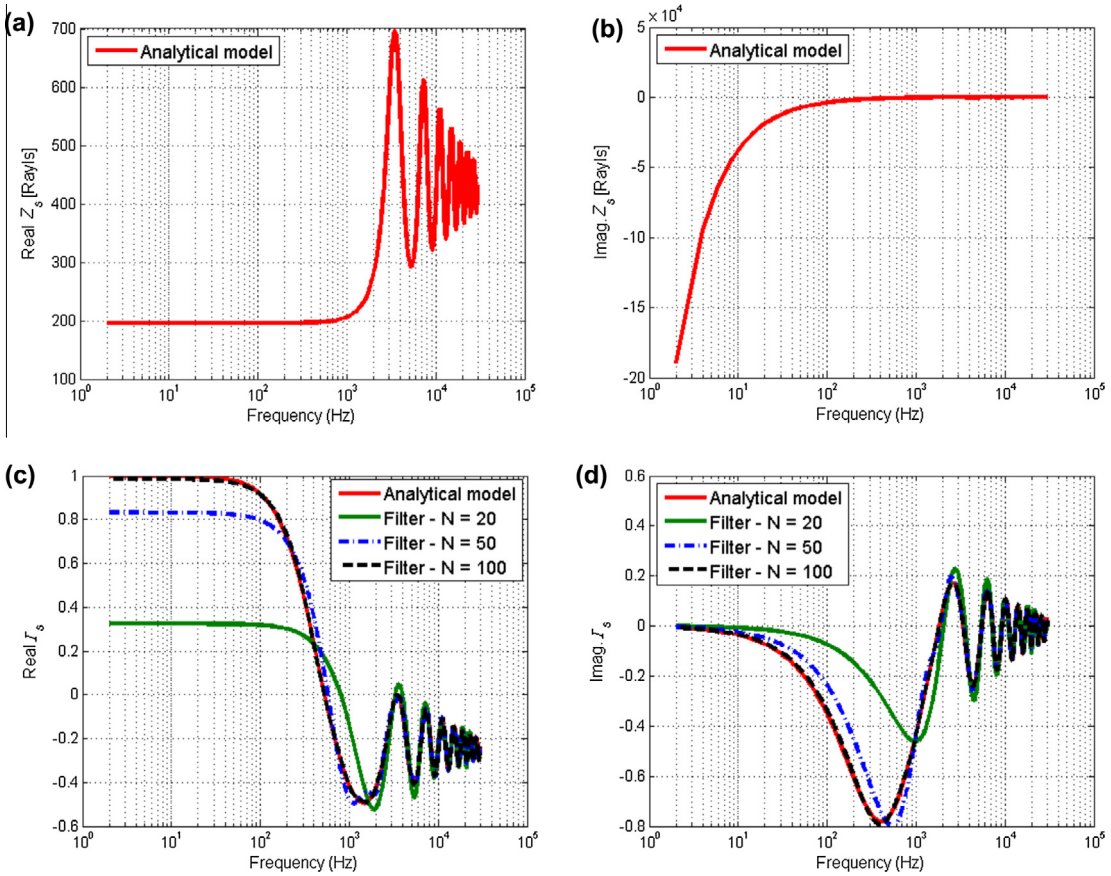

Fig. 11. Surface impedance and reflection factor in the frequency domain – melamine. (a) Impedance – real part, (b) impedance – imag. part, (c) reflection factor – real part and (d) reflection factor – imag. part.

amplitude. Therefore, increasing the spectral resolution, by increasing the time simulated, tends to reduce the shift in the resonance frequency and amplitude, as can be clearly observed in Fig. 8.

In the next sections, two types of sound absorbing materials are used as boundary conditions, a fictitious one and melamine, to validate the FIR filter representation of complex impedance. For both materials, the results obtained by FEM–FD (Comsol v4.3) and DHM–TD (Matlab® algorithm) numerical methods were compared.

4.3. FIR filter – Fictitious Material

The parameters tortuosity of 1.5, porosity of 20%, flow resistivity of 100,000 N s/m^4 and sample thickness of 0.02 m were used to obtain the real and imaginary parts of the surface impedance and applied in FEM–FD simulations, as well as the complex reflection factor values were calculated based on Eq. (22) and used as input data for the calculation of the FIR coefficients in the time domain, required for the DHM–TD simulation.

Figs. 9 and 10a show the convergence of the material surface impedance Z_s, reflection factor Γ_s and absorption coefficient values for three different filter orders ($N = 20$; $N = 50$; $N = 100$). In this case, larger errors can be seen only when using 20 coefficients in the filter. The impact of the errors observed in Fig. 10a can be seen in Fig. 10b, which shows the cavity frequency response obtained using the FEM–FD model and the DHM–TD for the three different options of filter coefficients. Overall, a good agreement can be observed, even for the DHM–TD simulation with only 20 coefficients. Small errors can be noted for frequencies below 200 Hz with the reduced number of filter coefficients, which is to be expected considering the behavior of the absorption coefficient curve. However, the use of an FIR filter with 50 coefficients is sufficient to ensure a very good agreement between the curves.

The result's accuracy is dependent on a number of factors, notably the filter type and mathematical technique used to calculate the coefficients, as well as the selected filter order. If the impedance curve in the frequency domain has a smooth variation, it can be expected that relatively low-order filters are able to accurately represent the material behavior in a time domain simulation. In order to verify this, another material is analyzed in the next section, which has an absorption coefficient that includes the whole transition behavior in the frequency range of interested.

4.4. FIR filter – melamine

Simulations similar to those described in the previous section were carried out considering the sound absorbing material melamine, which is commonly used in acoustic treatments. Surface impedance values (Z_s) were also obtained applying Eq. (22), although in this case the input parameter values were estimated based on experimental data obtained in [37], where the methods for the characterization of sound absorbing materials were presented. In the mentioned work, the experimental procedures to obtain porous materials parameters, such as tortuosity, porosity, viscous and thermal characteristic lengths, and flow resistivity were implemented and described in detail.

The results presented very good agreement, which included for the case of melamine the values: tortuosity of 1.0, porosity of 99%, flow resistivity of 9500 N s/m^4 and sample thickness of 0.043 m. The impedance values are shown in Figs. 11a and 10b

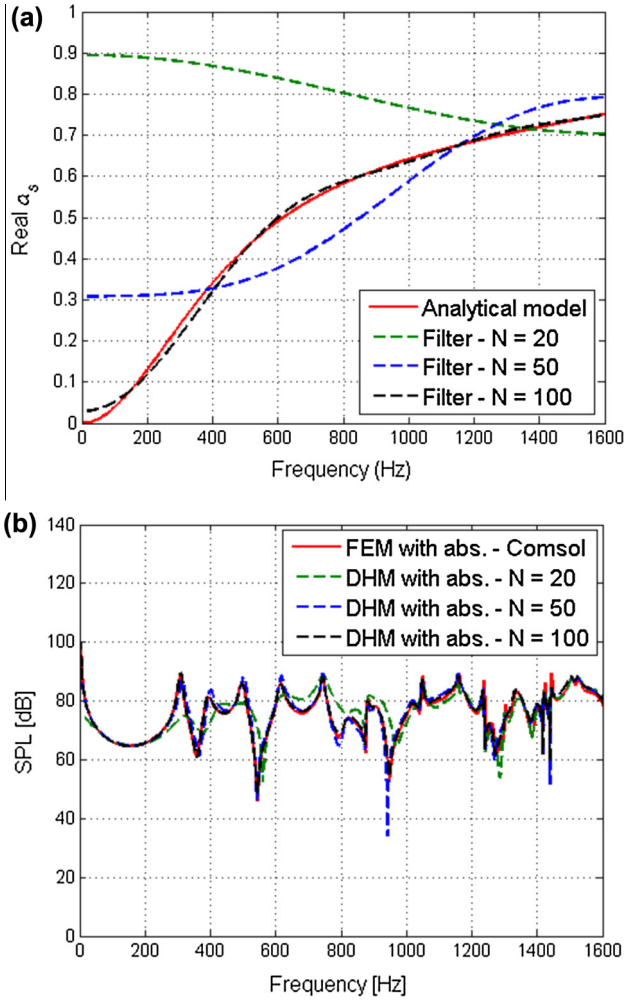

Fig. 12. Frequency response after application of melamine. (a) Absorption coefficient and (b) frequency response.

and the reflection factor values in Figs. 11c and 10d, and these were applied to the upper face of the cavity as described in the previous section.

Fig. 12a shows the absorption coefficient values and Fig. 11b the cavity frequency response after applying the FIR filter. It is possible to identify significant differences among the filter orders, especially for $N = 20$, which clearly shows that for the melamine, the reflection factor curve varies in a more significant way than in the case of the fictitious material.

As can be observed, the higher the filter order the better the agreement with results from other techniques will be. Although higher filter orders become necessary to adequately describe the melamine behavior in the time domain, the DHM3D-FIR algorithm presents considerably better computational performance than FEM–FD simulations (Ref. Table 3) and still remains at a reasonable limit for practical applications.

Table 3
Simulation synthesis – with wall absorption for both materials.

Parameters	Values
Simulation time	0.5 s
Time step (Δt)	$\cong 1.68 \times 10^{-5}$ s
Number of iterations	29,741
Cut-off frequency	3434 Hz
Frequency step (Δf)	2 Hz
CPU time	DHM (N = 20) ≅ 290 s
	DHM (N = 50) ≅ 295 s
	DHM (N = 100) ≅ 305 s
	FEM ≅ 16,200 s

Note: Intel processor Core (TM) i7 CPU @ 2.93 GHz 6 GB RAM, Windows 64 bits.

It is important to note that the DHM convolution algorithm can incorporate models where the reflection factor is dependent on other variables such as the angle of incidence. The incident angle could be incorporated in the model by using a different type of node, with more branches pointed in different angles. For each angle a different set of filter coefficients should be applied. However, for the presented analysis, it is assumed that the influence of this variable is rather small. Likewise, it is considered that the materials can be defined as locally-reactive.

In summary, the key concept of the procedure consists of obtaining, through efficient mathematical techniques of filter design, coefficients able to adequately describe frequency-dependent materials in a time domain simulation.

5. Conclusions

In this study, a DHM–TD implementation of boundary reflection factor values in the time-domain has been proposed. The reflection factor may present a set of values related to the material impulse response, which allows a multi-frequency analysis. These values were applied in the DHM–TD algorithm using FIR digital filter coefficients.

Two different materials were considered using as reference data the frequency response obtained from FEM–FD simulations. In both cases, the results present a very good level of agreement, with a great advantage associated with DHM–TD in terms of processing time. Based on these results, it can be concluded that this approach can be successfully applied to the modeling of the reflection factor in the time domain.

Other techniques based on analytical models in the time domain and also Infinite Impulse Response (IIR) filter design should also be explored in order to investigate solutions that could produce better results both in terms of impulse response quality and computational cost. The subject of filter design considered in this paper, can be very complex and requires special attention by the researcher, allowing many future studies to be developed.

Acknowledgements

This work was funded by CAPES – Coordenadoria de Aperfeiçoamento de Pessoal de Nível Superior and CNPq – Conselho Nacional de Desenvolvimento Científico e Tecnológico. The authors would like to thank the researches Eric B. Carneiro (UFSM) and Paulo H. Mareze (UFSM) for the valuable contributions.

References

[1] Christian Huygens. Traité de la lumière. GAUTIIIER-VILLARS ET CIE, Ed. Paris; 1920.
[2] Johns Peter B, Beurle Raymond L. Numerical solution of 2-dimensional scattering problems using a transmission-line matrix. Proc Inst Electr Eng 1971;118:1203–8.
[3] Kagawa Y, Tsuchiya T, Fujii B, Fujioka K. Discrete Huygens' Model approach to sound wave propagations. J Sound Vib 1998;218(3):419–44.
[4] Patankar Suhas V. Numerical heat transfer and fluid flow. In: Phillips Mary A, Millmann Edward M, editors. Taylor & Francis; 1980.
[5] de Cogan Donard, O'Connor William J, Pulko Susan. Transmission line matrix (TLM) in computational mechanics. CRC Press Inc.; 2005.
[6] Christopoulos Christos. The transmission-line modeling method: TLM. In: Dudley Donald G, editor. Wiley-Blackwell; 1995.
[7] Trenkic V, Christopoulos C, Benson TM. Simple and elegant formulation of scattering in TLM nodes. Electron Lett 1993;29(18):1651–2.
[8] Herring Jonathan L. Developments in the transmission-line modelling method for electromagnetic compatibility studies. University of Nottingham; 1993.
[9] Christopoulos Christos. The transmission-line modeling (TLM) method in electromagnetics. Synth Lectures Comput Electromagnetics 2006;1(1):1–132.

[10] Kuttruff Heinrich. Room acoustics. 4th ed. London, England: Taylor & Francis; 2000.
[11] Hofmann Jan, Heutschi Kurt. Simulation of outdoor sound propagation with a transmission line matrix method. Appl Acoust 2007;98:158–72.
[12] Carvalho RST. Modelo Físico de Huygens na solução discretizada de campos acústicos (Huygens physical model for the discretized solution of acoustic fields). Universidade Federal de Santa Catarina, Florianópolis, Ph.D. Thesis; 2013.
[13] Guillaume Gwenaël, Picaut Judicaël, Dutilleux Guillaume, Gauvreau Benoît. Time-domain impedance formulation for transmission line matrix modelling of outdoor sound propagation. J Sound Vib 2011;330:6467–81.
[14] Tsuchiya Takao. Numerical simulation of sound wave propagation with sound absorption using digital Huygens' model. Jpn J Appl Phys 2007; 46(7B):4809–12.
[15] Konrad, Walstijn, van Kowalczyk Maarten. Formulation of locally reacting surfaces in FDTD/K-DWM modelling of acoustic spaces. Acta Acustica United Acustica 2008;94:891–906.
[16] Bezdek M, Zhu Hao, Rieder A, Drahm W. Transmission line matrix modeling of sound wave propagation in stationary and moving media. In: Bock Hans-Georg, et al., editors. Progress in industrial mathematics at ECMI 2004, vol. 8. Berlin Heidelberg: Springer; 2006. p. 315–9. doi: http://dx.doi.org/10.1007/3-540-28073-1_50.
[17] Guillouard K, Wong MF, Fouad Hanna V, Citerne J. Comparison of the transmission-line matrix and finite-difference time-domain methods for a problem containing a sharp metallic edge. IEEE Trans Microw Theory Tech 1999;47(10):2042–5.
[18] Eswarappa Channabasappa, Hoefer Wolfgang JR. Bridging the gap between TLM and FDTD. IEEE microwave and guided wave letters, vol. 6, no. 1; 1996. p. 4–6.
[19] Krumpholz Michael, Huber Christian, Russer Peter. A field theoretical comparison of FDTD and TLM. IEEE Trans Microw Theory Tech 1995; 43(8):1935–50.
[20] Tsuchiya T, Hara T, Tsuji T, Kagawa Y. Discrete Huygens' modelling simulation of sound wave propagation in velocity varying environments. J Sound Vib 2001;246:419–39.
[21] Guillaume G, Aumond P, Gauvreau B, Dutilleux G. Application of the Transmission Line Matrix Method for outdoor sound propagation modelling – Part 1: model presentation and evaluation. Appl Acoust 2014;76:113–8.
[22] Choi Dok Hee, Hoefer Wolfgang JR. The simulation of three dimensional wave propagation by a scalar TLM model. IEEE MTT-S DIGEST; 1984. p. 70–1.
[23] Tizianel Julian, et al. Transport parameters and sound propagation in an air-saturated sand. J Appl Phys 1999;86.
[24] Vorländer Michael. Auralization: fundamentals of acoustics, modelling, simulation, algorithms and acoustic virtual reality, 1st ed. RWTH, Ed., vol. 1 Aachen: Springer; 2007.
[25] Dalla'Rosa A. Modelagem e Otimização da Localização de Transmissores em Ambientes Internos de Comunicação Sem Fio (3D numerical modelling of electromagnetic compatibility problems using the TLM-TD method). Universidade Federal de Santa Catarina, Universidade Federal de Santa Catarina, Florianópolis; 2008.
[26] Rossing Thomas D. Propagation of sound. In: Handbook of acoustics. New York: Springer; 2007. p. 60–61.
[27] Chobeau Pierre, Dutilleux G, Picaut J, Ecotière D. PML implementation for the TLM propagation model in acoustics. In: AIA-DAGA 2013 conference on acoustics, Italy; 2013.
[28] Shin Kihong, Hammond Joe. Fundamentals of signal processing for sound and vibration engineers. John Wiley & Sons Ltd.; 2008.
[29] Bilbao Stefan. Wave and scattering methods for numerical simulation. Wiley; 2004.
[30] Oppenheim Alan V, Schafer Ronald W. Discrete-time signal processing. In: Oppenheim Alan V, editor. Prentice-Hall Inc.; 1989.
[31] Allard JF, Atalla N. Propagation of sound in porous media. 2nd ed. Chichester, United Kingdom: John Wiley & Sons Ltd.; 2009.
[32] Johnson DL, Koplik J, Dashen R. Theory of dynamic permeability and tortuosity in fluid-saturated porous media. J Fluid Mech 1987;176:379–402.
[33] Lafarge D, Lemarinier P, Allard J, Tarnow V. Dynamic compressibility of air in porous structures at audible frequencies. J Acoustical Soc Am 1997;102:1995.
[34] Moler Cleve B. Least squares. In: Numerical computing with MATLAB. The Mathworks Inc.; 2004. p. 141–59.
[35] Kagawa Y, Tsuchiya T, Fujioka K, Takeuchi M. Discrete Huygens' Model approach to sound wave propagations–reverberation in a room, sound source identification and tomography in time reversal. J Sound Vib 1999;225(1):61–78.
[36] Douglas D. Reynolds, engineering principles of acoustics: noise and vibration control. Boston: Allyn and Bacon Inc.; 1981.
[37] Paulo Henrique Mareze. Análise da influência da microgeometria na absorção sonora de materiais porosos de estrutura rígida (Analysis of the microgeometry influence in the sound absorption of a porous rigid structure). Florianópolis: Universidade Federal de Santa Catarina; 2013.